






RESEARCH PAPER



A multi-scalar climatological analysis in preparation for extreme heat at the Tokyo 2020 Olympic and Paralympic Games

Jennifer K. Vanos ^a, Wendy Marie Thomas^b, Andrew J. Grundstein ^c, Yuri Hosokawa ^d, Ying Liu ^e, and Douglas J. Casa ^f

^aSchool of Sustainability, Arizona State University, Tempe, AZ, USA; ^bAcclimate Institute, Washington, DC, USA; ^cDepartment of Geography, University of Georgia, Athens, GA, USA; ^dFaculty of Sport Sciences, Waseda University, Tokorozawa, Japan; ^eDepartment of Environmental and Occupational Health, University of Montreal, Montreal, Canada; ^fKorey Stringer Institute, Department of Kinesiology, University of Connecticut, Storrs, CT, USA

ABSTRACT

Extreme heat can be harmful to human health and negatively affect athletic performance. The Tokyo Olympic and Paralympic Games are predicted to be the most oppressively hot Olympics on record. An interdisciplinary multi-scale perspective is provided concerning extreme heat in Tokyo—from planetary atmospheric dynamics, including El Niño Southern Oscillation (ENSO), to fine-scale urban temperatures—as relevant for heat preparedness efforts by sport, time of day, and venue. We utilize stochastic methods to link daytime average wet bulb globe temperature (WBGT) levels in Tokyo in August (from meteorological reanalysis data) with large-scale atmospheric dynamics and regional flows from 1981 to 2016. Further, we employ a mesonet of Tokyo weather stations (2009–2018) to interpolate the spatiotemporal variability in near-surface air temperatures at outdoor venues. Using principal component analysis, two planetary (ENSO) regions in the Pacific Ocean explain 70% of the variance in Tokyo's August daytime WBGT across 35 years, varying by 3.95°C WBGT from the coolest to warmest quartile. The 10-year average daytime and maximum intra-urban air temperatures vary minimally across Tokyo (<1.2°C and 1.7°C, respectively), and less between venues (0.6–0.7°C), with numerous events planned for the hottest daytime period (1200–1500 hr). For instance, 45% and 38% of the Olympic and Paralympic road cycling events (long duration and intense) occur midday. Climatologically, Tokyo will present oppressive weather conditions, and March–May 2020 is the critical observation period to predict potential anomalous late-summer WBGT in Tokyo. Proactive climate assessment of expected conditions can be leveraged for heat preparedness across the Game's period.

ARTICLE HISTORY

Received 11 December 2019
Revised 5 February 2020
Accepted 6 February 2020

KEYWORDS

Tokyo; extreme heat; ENSO; wet bulb globe temperature; athletes

Introduction


The Summer Olympic Games in Tokyo, 2020

The Tokyo 2020 Olympic and Paralympic Games will be held from July 24 to August 9 and August 26 to September 6, respectively. The Games will incorporate 33 events, 43% of which will take place outdoors within the Greater Tokyo Area, Tokyo Bay, and Sapporo. Tokyo is the world's most populous mega-city at 13.6 million people. It lies in a humid subtropical climate zone with hot, humid summers and generally mild winters. Japan's climate has endured steady and noticeable changes, owing both to climate variance (natural influences) and climate change (anthropogenic) [1,2]. July and August are the warmest, most

humid, and wettest months, with a noticeable convective shift often occurring in early August, bringing more intense heat and humidity [3].

The growing international audience for the Summer Olympics now exceeds 3.5 billion viewers over the 4 weeks [4]. While the late-July through September timeline may gain heightened international viewership (due to a “lull” in the North American sports schedule), extreme heat is a critical concern for athlete performance and health, as well as for workers, volunteers, and spectators alike. Further, Tokyo can expect an influx of >500,000 foreign travelers given numbers recorded at the Rio 2016 Games, and non-acclimatized spectators will be at a higher risk of heat stress [5].

CONTACT Jennifer K. Vanos  jvanos@asu.edu

 Supplemental data for this article can be accessed [here](#).

© 2020 Informa UK Limited, trading as Taylor & Francis Group

For most outdoor sports, spectators are likely to be standing or sitting in crowded, often unshaded areas, with large crowds causing decreased airflow [6] and higher temperatures due to metabolic heat [7]. Athletes will also need to heat acclimate or acclimatize and take extra precautions when preparing for outdoor events, particularly longer events such as football, road cycling, and tennis [8,9]. Given the climatologic (~30-year average) conditions in Tokyo in late summer (i.e. average daily maximum air temperatures of ~31°C), two of the longest endurance events—the race walk (50 km and 20 km) and the marathon—have been moved north to Sapporo to protect athletes and aid in performance.

Extreme heat & health in sports and mass gatherings

The concern over extreme heat at the impending Olympics is well known and ever-present in the media and recent literature (e.g. Smith et al. [10], Gerrett et al. [9]) Recent studies focus on the possibility of record summertime heat and humidity posing heat risks to many [11–13]. Apart from Mexico City and Rio de Janeiro, all past Summer Olympics were held in Temperate, Cold, or Mediterranean climates [14], yet few (<20%) of urban climate studies have addressed heat extremes in (sub) tropical regions [15]. Based on the humid climate, suggestions for the use of electric fans for forced ventilation for competition breaks or in spectator areas, and harnessing wind corridors in the city, can substantially aid in evaporative cooling from the skin and mixing of the air [16].

Paralympic athletes competing in Tokyo 2020 will also be exposed to these conditions. Forty-four hundred (4,440) athletes are expected to compete at the Paralympics across 22 sports [17]. The thermoregulation and performance of Paralympic athletes with impairments of spinal cord injury (SCI), cerebral palsy (CP), multiple sclerosis (MS), and amputees are compromised as compared to able-bodied athletes (see Griggs et al. [18] for a full review).

Predictions for heat preparedness

Advanced and accurate projections of the expected late-summer weather conditions across the region

and within the city can augment preparedness and ensure the provision of heat stress mitigation resources for athletes, spectators, volunteers, and coaches (e.g. Meehan et al. [19]). To further prevent heat-related illness (HRI) and improve preparedness, a climatologic risk assessment (a tool to help organizations identify their climate-related risks and thus improve event management strategies) is valuable to include in the planning of the Olympics, venue selection, and making informed decisions to avoid potential over-exposure to heat and thus HRI [8]. Researchers have yet to take a deeper look at the atmospheric drivers for probable thermal and moisture extremes (notably within the hotter/wetter regime) in Tokyo prefecture in late-summer 2020. Although select urban-scale heat studies in Tokyo have been presented (e.g. Honjo et al. [20] Matzarakis et al. [12]), none have connected planetary and regional extremes with local “hot spots” and event timing and duration.

Accordingly, the current paper connects past weather patterns indicative of the most extreme heat in Tokyo—including large-scale climatology, regional weather and climate, and intra-urban microclimates—to human health concerns of HRI and exertional heat illness (EHI). Specifically, we explore:

- Connections between historical regional (Tokyo metropolis) wet bulb globe temperature (WBGT) extremes and planetary ocean-atmosphere dynamics;
- Identification of local intraurban air temperature levels impacting specific venues in relation to duration and time of event.

These spatial scales combine to affect heat exposure of Olympic and Paralympic athletes competing in outdoor events at the Games. Our intention is to identify the planetary dynamics that best explain probable teleconnection to August weather in Tokyo. Since planetary dynamics start in the months and weeks prior to August 2020, they may be observed and used to support lead-time preparedness to aid athlete, worker, volunteer, and spectator safety. Specifically, the dynamics could indicate the *general tendency* for August to have “average” or “above/below” average heat and humidity. We first

provide a background and primer on the planetary climatology and teleconnections affecting Tokyo's late-summertime weather.

Climate background and overview: Tokyo, Japan

In recent years, the Japan Meteorological Agency (JMA) has reported above-normal air temperatures (T_a) (+0.5–1.5°C) in Tokyo in June, July, and August (JJA), with numerous recent studies investigating Japan's anomalous summer climate [3,21–23]. In particular, Enomoto et al. [3] and Wakabayashi and Kawamura [22] uniquely isolated August from the other summer months as the atmospheric dynamics exhibit a sharp turn from conditions in early summer (June–July). Enomoto et al. [3] describe this change as a “convective jump” that weakens the Baiu front of June–July, which gives rise to the Bonin High in eastern Japan. The Bonin/Ogasawara High (BOH) is

centered above the Ogasawara Islands 993 km (617 miles) southeast of Tokyo (see Figure 1) and is the predominant regional weather system in August. These high-pressure systems, in general, deliver higher T_a to Tokyo in August, and may also alter the direction of typhoons (e.g. will have to move around the high-pressure system), which tends to protect Tokyo from typhoons.

Planetary and regional climate dynamics

Local weather is a manifestation of planetary and regional climate dynamics interplaying with local geography (such as mountains and marine environments). The El Niño Southern Oscillation (ENSO) is one such interplay associated with Tokyo weather, which creates significant sea-surface temperature (SST) changes across a large swath of eastern and central Pacific (80°W–160°E, 5°N–5°S) (grey and blue equatorial regions of Figure 1). This particular swath of the Pacific Ocean is significant because its

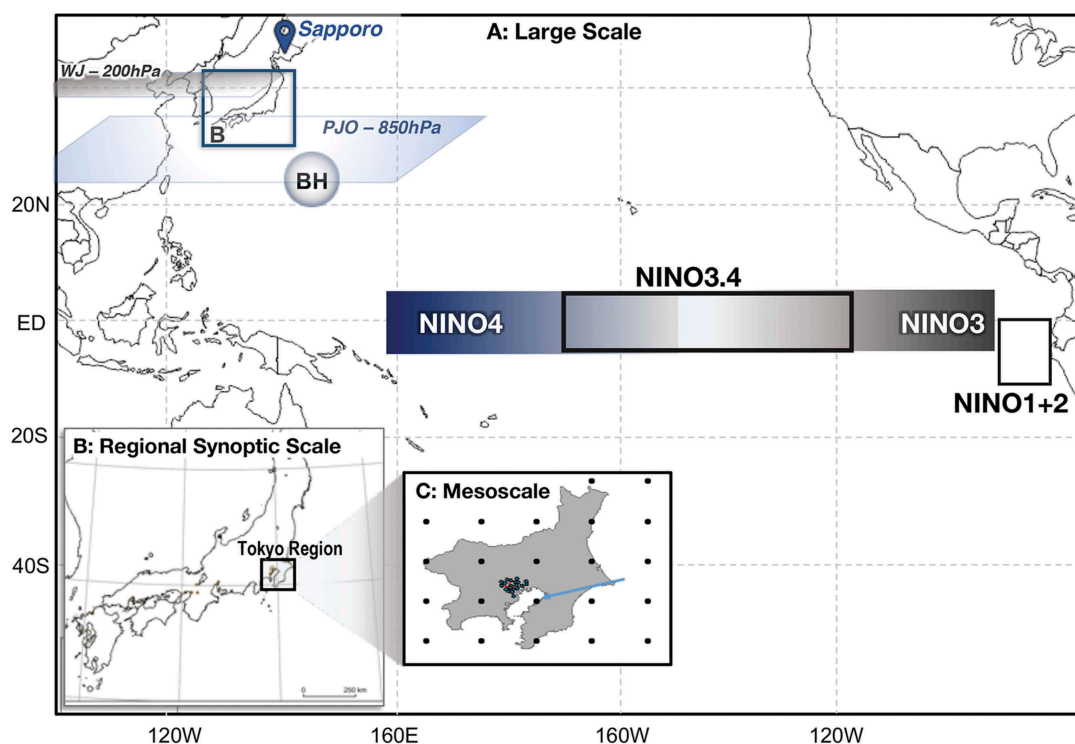


Figure 1. Overview of scales and atmospheric predictors affecting Tokyo's weather. (a) Large-scale (planetary) displaying Niño Regions. We used NINO3 and NINO3.4 in this study [Source: National Oceanic and Atmospheric Administration (NOAA, 2019), National Center for Environmental Intelligence (NCEI)]. (b) Synoptic scale – Country of Japan. (c) Regional scale showing MERRA-2 grid boxes over the Tokyo region at the meso-scale. BH, Bonin High. WJ (upper-level flow) and PJO (lower-level flow) also shown. See Figure 2 for intra-urban microscale and locations of venues within the city region. Conceptually, our large-scale analysis uses A, B, and C; the local microclimate was assessed separately in the current paper based on the weather station network to create Figures 4 and 5.

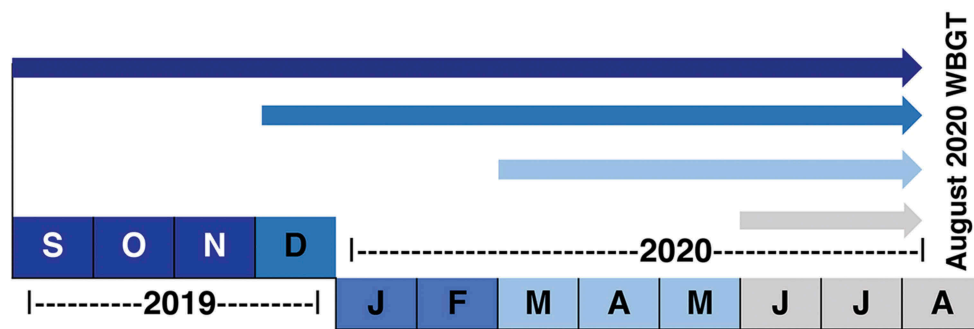


Figure 2. General timeline used within the current study to relate prior months of the year to the WBGT levels experienced in Tokyo, based on El Niño Southern Oscillation (ENSO) seasons. SON: September, October, November (Season 1); DJF: December, January, February (Season 2); MAM: March, April, May (Season 3); JJA: June, July, August (Season 4).

atmosphere-oceanic dynamics are well known to influence weather in many localities across the planet, and hence it is well studied [24–27] and has attracted interest in the climate and health community [28,29]. This type of influence is called a teleconnection, defined as the “linkage between weather changes occurring in widely separated regions of the globe” (e.g. weather in New York, NY, USA can be influenced by SST in equatorial Pacific) [30].

ENSO itself is described based on 1) phase: a positive or negative oscillation (fluctuation), and 2) intensity: the intensity of the oscillation. Both phase and intensity are measured by SST anomalies (difference from normal) in the central and eastern tropical Pacific Ocean across a 3-month running mean. An El Niño signal, or positive phase (+), indicates warmer SSTs, while a La Niña signal, or negative phase (–), presents cooler SSTs. The cooler SSTs are caused by strong easterly trade winds that increase cold water upwelling in the eastern tropical Pacific. These winds also blow warm water west toward Asia, with implications of high air temperatures in ENSO regions, like eastern Japan. Thus, a strong La Niña year has historically brought warmer weather to Japan in late summer and a lower number of typhoons, as inferred by Nitta [31].

The intensity of each phase is designated based on the following SST anomaly (difference from normal) ranges:

- “Neutral” ($\pm 0.5^{\circ}\text{C}$);
- “Weak” ($\pm 0.5^{\circ}\text{C}$ to 0.9°C);
- “Moderate” ($\pm 1.0^{\circ}\text{C}$ to 1.4°C);
- “Strong” ($\pm 1.5^{\circ}\text{C}$ to 1.9°C);
- “Very Strong” ($\geq \pm 2.0^{\circ}$).¹

Hence, it follows that an El Niño (La Niña) would have higher (lower) SSTs compared to neutral conditions. Japan is also more sensitive to the La Niña phase weather patterns related to extreme heat events [21,32–34]. ENSO forms several months ahead of observed/analyzed teleconnection impacts [27,35]. Thus, given that Japan is in a known teleconnection area, understanding ENSO’s long-term relationship with Tokyo’s daytime WBGT levels in August, specifically, could lend predictive value for gauging the probable average and potential anomalous (lower or higher) heat levels during the Olympic and Paralympic Games.

The ENSO transition (known as the “spring predictability barrier”) occurs in March, April, and May (MAM) for the northern hemisphere, and is thus a critical time for predicting possible weather anomalies in late summer/early fall for teleconnection areas [36], such as Tokyo. Thus, the ENSO tendency is often announced by national weather services in MAM to forecast the rest of the ENSO year, which ends in August (see Supplemental Material). A review of observational data (e.g. ENSO phase and intensity) at that time could give more precise guidance for atmospheric tendencies (e.g. below, average, or anomalous warmth in Tokyo) for the Olympic and Paralympic period. Currently (as of March, 2020), neutral conditions are persistent in the equatorial Pacific. These conditions are favored through spring 2020 (~65% chance), and are expected to continue through summer 2020 (55% chance) [37]. The latest probabilistic models also show a strongly enhanced probability (70%) for above normal 2 m air temperatures and SSTs in July in Japan [38] (see also Supplemental Material).

ENSO regions, regional dynamics, and Tokyo weather

Here, we draw attention to the ENSO regions of NINO3 and NINO3.4 (Figure 1). NINO3 is the original zone of study for teleconnection patterns. In the mid-to-late 1990s, the NINO3.4 zone further west (which adjoins portions of NINO3 and NINO4) demonstrated even greater teleconnection correlations [35]. The Pacific Japan Oscillation (PJO)—an atmospheric near-surface flow (850hPa) located southeast of Japan—is coupled with ENSO and has also been shown to influence Japan’s weather [31,33] and may contribute to local Tokyo weather (see Table 1). A positive PJ index (PJI) is associated with La Niña (and thus generally hotter more humid air conditions in Tokyo) and a negative PJI is associated with El Niño (cooler air conditions) [21].

An upper-level (200hPa) fast-moving wind—the West-Asia Jet (WJ)—located to the west of Japan—is also linked to ENSO, yet the physical relationship requires further research [3]. The WJ is an outflow from atmospheric processes further east and is associated with the Asian/Indian Monsoon [3,39]. In eastern Japan, higher air temperatures are shown to be positively influenced by the PJO [22]. Finally, air–sea interactions that develop from ENSO can influence Rossby wave excitation, which is a significant planetary wave that can modulate regional circulations such as the WJ

and PJO [40]. Detailed descriptions of PJO and WJ indices, and further ENSO information, are found in Table 1 and Supplemental Material.

Methodology

The methods herein are presented from large-scale (planetary) to regional and small-scale (urban) influences on Tokyo’s late summer weather. While hot and humid conditions are expected given Tokyo’s climate, planetary-to-regional weather patterns/teleconnections may cause even worse (or better) conditions. By analogy, our approach is akin to initiating a gym “battle rope” (e.g. ENSO) and observing how it “activates” other points (or nodes) (e.g. the PJO or WJ) downstream, which in turn can influence local Tokyo WGBT. Unlike the rope, however, the atmosphere is highly non-linear, yet these principles apply. At a fine-scale, urban design may result in higher or lower localized temperature, humidity, and radiative loads affecting athletes, spectators, workers, and volunteers.

The City of Tokyo and the 2020 Olympic and Paralympic Games

August is the predominant month for competition for both Olympic and Paralympic events and is thus the temporal focus of this study. Tokyo prefecture

Table 1. Descriptions of the Pacific Japan Oscillation (PJO) and West-Asia Jet (WJ)—critical regional factors linked to the El Niño Southern Oscillation (ENSO) as climate forcings. The connections of these forcings to “extraordinary” summers (hot or cool) in Japan are also described in the final column.

Teleconnection	Description	Relationship to Tokyo’s weather
Pacific Japan Oscillation (PJO) ^a	An atmospheric surface-flow that occurs at the 850hPa (near surface) level, with a general height range between 1.2 and 1.6 km above sea-level. The PJO is typically centered near the Philippines and contributes to the northward migration of tropical cyclones. The PJO pattern can intensify the Bonin/Ogasawara High, but does not explain its existence, only its variability in strength [3]. <ul style="list-style-type: none"> • Positive PJO → La Niña phase^b • Negative PJO → El Niño phase^b • Positive August PJO → enhanced typhoon/cyclone activity^b [23]. 	<ul style="list-style-type: none"> • More hot and humid conditions are likely during La Niña years, owing (in part) to the ENSO-PJO dynamic. • Positive PJO supports warmer and more humid air in eastern Japan [23]. • Hot summers overall [22].
West-Asia Jet (WJ)	An atmospheric upper-level fast-moving flow at the 200 hPa level, with a general height range of 10–12 km above sea-level (the typical “cruising altitude” of a long-distance flight). The WJ mainly develops, in part, from excitations in the Indian Ocean, where atmosphere/ocean and land interactions influence an upper-air regional flow in western Asia [41].	<ul style="list-style-type: none"> • More significant in explaining the formation of the August high-pressure system [3]. • Positive WJ enhances the Bonin/Ogasawara High → higher temperatures in eastern Japan [3].

^aPacific Japan (PJ) is often used as an abbreviation for PJO. The oscillation is measured as the Pacific Japan Index (PJI).

^bAlthough studies have demonstrated these links, Tsuyuki and Kurihara [42] found no clear link between ENSO and the PJO.

(139°E, 35°N) is the specific spatial focus, although the marathon and race walk were moved north to Sapporo (141°E, 43°N). The average high/low temperature in Tokyo in August is 31/24°C (26/19°C for Sapporo). When combined with intense relative humidity (RH, averaging 73% in August) (e.g. Figure 6 for daytime RH and T_a variations), Tokyo's heat index reaches an average August value of 38.3°C (101°F). Tokyo further experiences ~5.8 tropical storms on average in August, which can affect water conditions (temperature, pollution) [43].

The 2020 Olympics and Paralympics will consist of 33 and 22 sporting events, respectively, across 43 venues (26 outdoor) (Table 2). Most locations are within the greater Tokyo area, with locations mapped in Figure 2. However, specific

Table 2. Venue name and number for each sport corresponding to Figure 3. Note most outdoor Paralympic venues match that of the Olympic venues for the corresponding sport apart from venue 26.

Venue No.	Sport	Venue name/location
1	Swimming marathon	Odaiba Marine Park
2	Archery	Yumenoshima Park Archery Field
3	Athletics	Olympic Stadium
4 ^a	Race walk	Sapporo, Japan
5 ^a	Marathon	Sapporo, Japan
6	Baseball/Softball	Yokohama/Fukushima Azuma stadium
7	Canoe Slalom	Kasai Canoe Slalom Centre
8	Canoe & Kayak Sprint	Sea Forest Waterway
9	Cycling (BMX)	Ariake Urban Sports Park
10 ^b	Cycling (Mtn Bike)	Izu MTB Course
11 ^b	Cycling (Road)	Fuji International Speedway
12	Equestrian	Equestrian Park
13a–f	Football	13a Tokyo Stadium 13b ^b Kashima Stadium 13c ^b Miyagi Stadium 13d Saitama Stadium 13e ^b Yokohama Int. Stad. 13f Olympic Stadium (venue 3)
14 ^b	Golf	Kasumigaseki Country Club
15	Hockey	Oi Hockey Stadium
16	Mod. Pentathlon	Tokyo Stadium & Musashino Forest Sports Plaza
17	Rowing	Sea Forest Waterway
18	Rugby	Tokyo Stadium
19	Sailing	Enoshima Yacht Harbour
20	Shooting	Asaka Shooting Range
21	Skateboarding	Ariake Urban Sport Park
22 ^b	Surfing	Tsurigasaki Surfing Beach
23	Tennis	Ariake Tennis Park
24	Triathlon	Odaiba Marine Park
25	Beach Volleyball	Shiokaze Park
26	Football 5-a-Side	Aomi Urban Sports Park

^a Events moved to Sapporo Japan. ^b Events not shown on map; outside of grid boundaries.

venues (e.g. marathon, race walk, cycling, golf) are far from the city center.

Meteorological and climatological data sources

Each spatial scale of data used herein is presented in Figures 1 and 2. Below, we first address the large-scale planetary dynamics methods (*Large-Scale Climatology & Teleconnections*) (encompassing teleconnections across the Pacific Ocean). Second, we examine regional dynamics using re-analysis meteorological data (*MERRA-2 data*). Finally, intraurban microscale temperatures across Tokyo are assessed with ground-based weather station data (*Micrometeorological station data for intra-urban mapping*). These spatial scales provide an in-depth, multi-scale exploration of the projected heat extremes in Tokyo in August 2020. The temporal scales analyzed are described in each section.

Large-scale climatology & teleconnections

Given that specific features of ENSO (PJO/La Niña) have been linked to anomalous higher temperatures and humidity in Japan [21–23,33], we assess the associations between ENSO and how its characteristics lend to probable thermal and moisture extremes in Tokyo's summers—notably within the hotter/wetter regime—and thus a higher or lower WBGT. ENSO data, specifically NINO3 and NINO3.4, were sourced from the NOAA/NCEP Climate Prediction Center (2019) [44]. Geopotential height anomaly data at 850hPa and 200hPa were obtained from the NCAR/NCEP global Reanalysis I dataset [45], and were normalized to 1981–2010 climate average. The 850hPa data were used to calculate the PJI, and the 200hPa data were used to calculate the WJ Index (WJI).

To identify the ranking and strength for ENSO within region NINO3.4, we utilized the NOAA Earth System Research Laboratory's (ESRL) "Top 24 strongest El Niño and La Niña events by season, 1895–2015" [46]. We also used the Indian Institute of Tropical Meteorology's "Interannual Variations of Indian Summer Monsoon" dataset to obtain significant monsoon flood and drought years from 1871 to 2015, as monsoon activity can impact the WJ [47].

Finally, we caution that while we earlier reference to the BOH, we did not directly study the BOH, as the WBGT is more hyper-local and

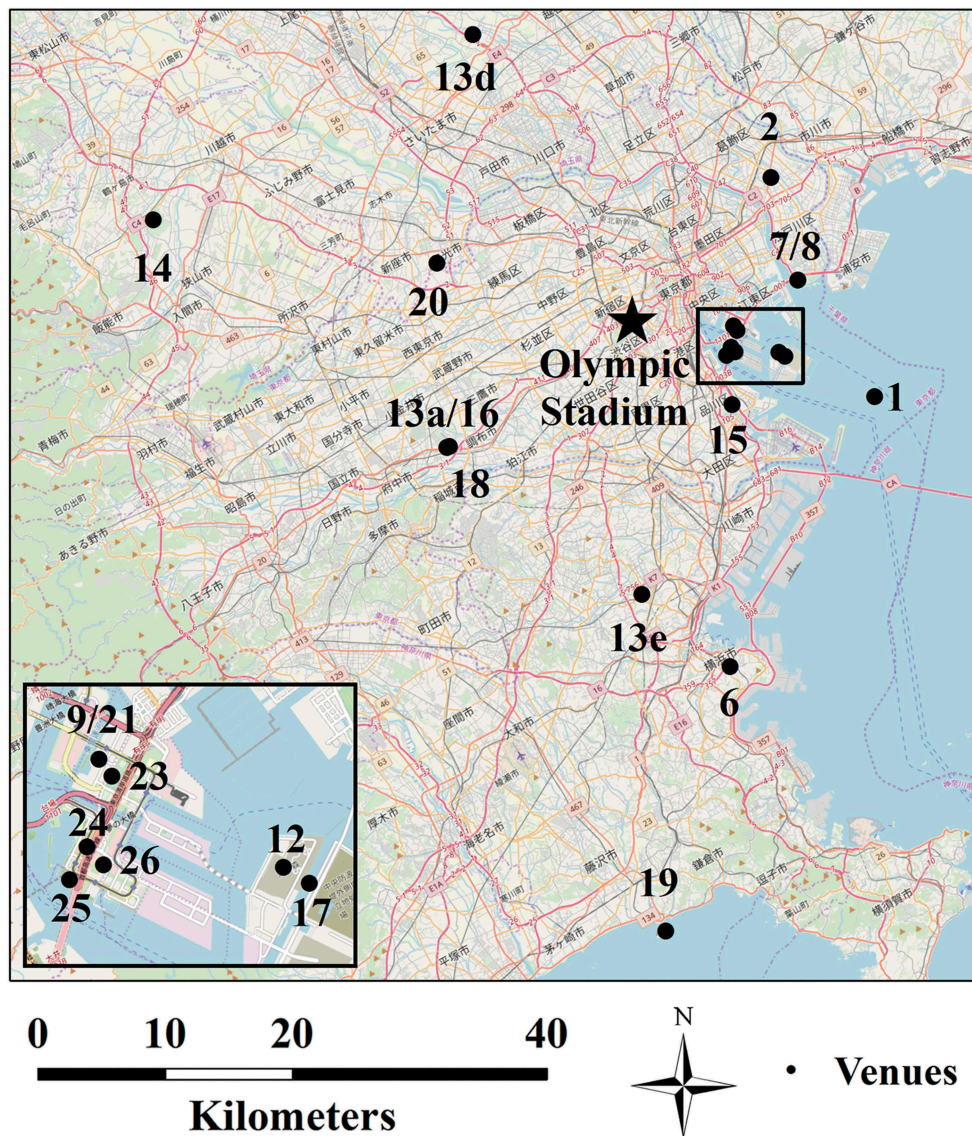


Figure 3. Tokyo map of outdoor venue locations. See Table 2 for venue names and sports at each location.

pertinent to those attending the Games. In some ways, however, the WGBT is a pseudo-proxy for the BOH intensity since it is a comprehensive heat metric that includes other factors that are also related to high-pressure systems (e.g. high air temperature, low winds, high solar radiation/lack of clouds).

MERRA-2 data

Hourly meteorological data (T_a , RH, windspeed, and solar radiation) were obtained from the second Modern-Era Retrospective Analysis for Research and Applications (MERRA-2) of 1980–2016 [48]. MERRA-2 is a National Aeronautics and Space Administration (NASA)-developed atmospheric

reanalysis dataset that provides global data at a $0.6258^\circ \times 0.58^\circ$ longitude-by-latitude resolution. Further, MERRA-2 provides a complete long-term record needed for our comparison with ENSO.

We selected the grid cell located nearest to Tokyo (grid centroid 35.5°N , 140°E). The maximum daytime WGBT values (*Wet bulb globe temperature heat metric*) match closely with ground-based station data (see Supplemental Material). We further integrate the MERRA-2 WGBT data for daylight hours (~0500h–1900h) with the climatological indices (ENSO, PJI, WJI, and WGBT) to perform principal component analysis (PCA) given the temporal compatibility between datasets within a climatological time frame (20–30 years).

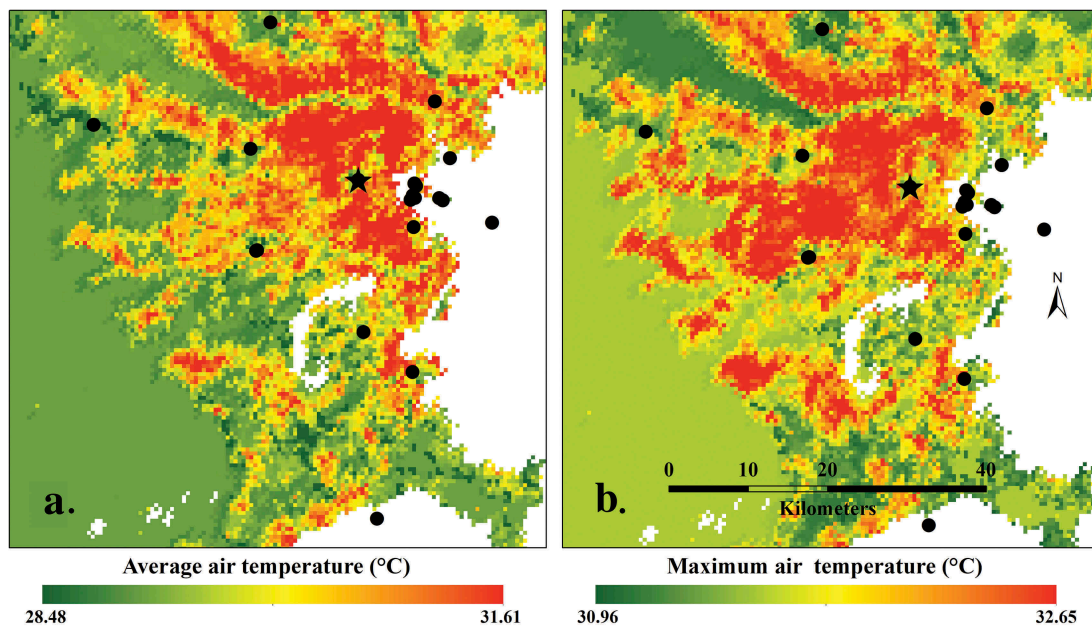


Figure 4. Intraurban temperature variability of “daytime” (0500–1900 hr) air temperatures at a 500 m scale, showing (a) average across the day, and (b) average of the maximum daytime air temperatures, for August 2008–2018 in the Tokyo region using random forests-based regression kriging (RFRK). Circles indicate venue numbers and star is Olympic stadium (see Table 2 & Figure 3 for reference). To clearly show the spatial variations between Figures 4 and 5, the scales of mean temperature and the scales of max temperature are matched.

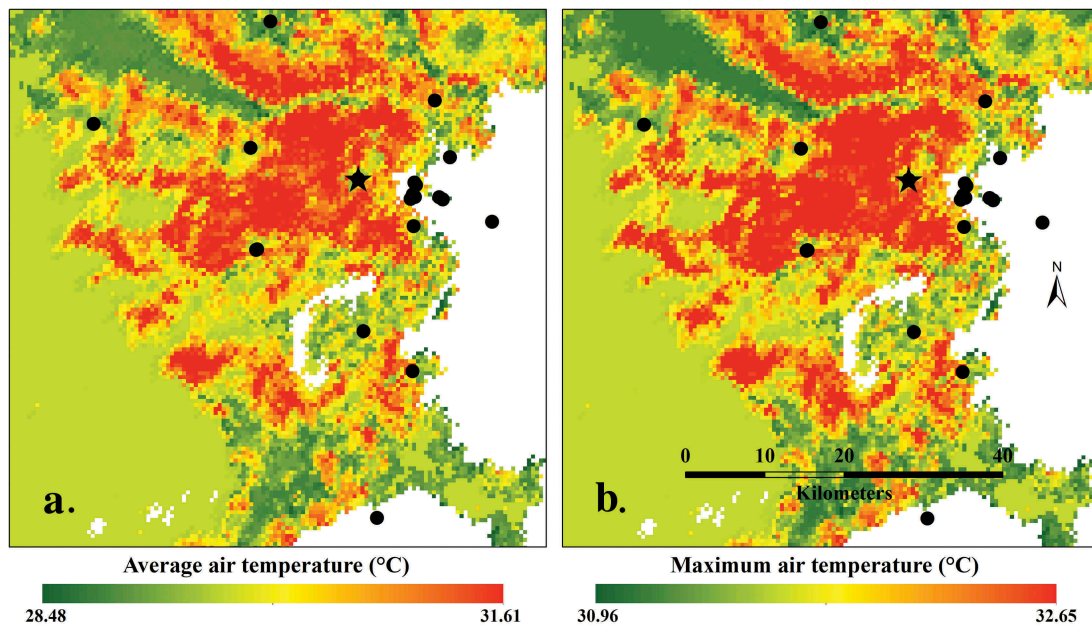


Figure 5. Intraurban temperature variability of midday (1200–1500 hr) air temperatures, showing (a) average across the 3-hr period, and (b) average of the maximum within the 3-hr period, for August 2008–2018 in the Tokyo region using random forest-based regression kriging (RFRK). Circles indicate venue numbers and star is Olympic stadium (see Table 2 & Figure 3 for reference).

Micrometeorological station data for intra-urban mapping

Hourly August T_a and RH data were obtained from 24 stations within the Tokyo metropolis from two sources for 2008–2018:

- (1) The Air Quality Monitoring System (AQMS), which provides both RH and T_a . The AQMS network continuously measures meteorological parameters and air pollution using sensors from HORIBA, Ltd.

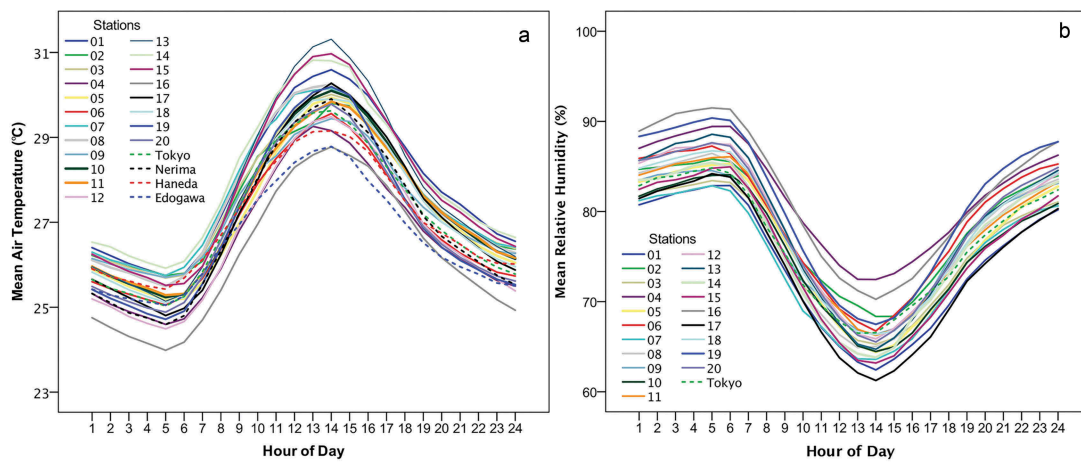


Figure 6. (a) Mean air temperature and (b) and relative humidity diurnally for August across 10 years (2009–2018) from AQMS stations (20) and AMEDAS stations (4).

(2) The Automated Meteorological Data Acquisition System (AMeDAS). The AMeDAS network is a collection of ~1300 Automatic Weather Stations (AWSs) run by the JMA in collaboration with the WMO for weather observations to support real-time monitoring of weather conditions with high temporal and spatial resolution [49]. We also used an AMeDAS station from Sapporo. The AMeDAS stations employ Meisei Electric Co. Ltd. Sensors [50,51].

Note that these stations do not measure solar radiation and thus WBGT was not calculated in the intra-urban analysis.

Data analysis for large-scale prediction of extreme heat

Wet bulb globe temperature heat metric

The WBGT will be used by the International Olympic Committee (IOC) for heat protection in athletes at Tokyo 2020. Meteorological inputs from MERRA-2 data were used to compute the Tokyo-wide (mesoscale, Figure 1, box C) daytime average WBGT using the Liljegren et al. [52] model, with inputs of T_a , RH, windspeed, and solar radiation to calculate the T_g and T_w , as follows:

$$\text{WBGT} = 0.7T_g + 0.2T_w + 0.1T_a \quad (1)$$

The Liljegren model has been extensively tested in a variety of climates, including humid subtropical,

and found to be accurate to within 1°C [52,53]. The WBGT is a “first approximation of heat stress” [54], and is designed to capture the various meteorological influences on heat stress, including radiant heat, vapor pressure, T_a , and windspeed, and is thus a more comprehensive indicator of heat stress than T_a alone [55]. However, it is important to note that while the use of WBGT is widespread, it is not without limitation (e.g. accounting for very high humidity, clothing) [54,56], and does not always respond like the human body, as a heat strain index would. It was specifically designed in a hot and humid climate to limit heat illness and death during activity (military, athletes, etc.) [57–59] and is a widely used metric in the global athletic community [8,60–62].

For Tokyo in August, the relevant WBGT activity modification and associated risk thresholds from existing literature for athletes are: 25.7–27.8°C “risk for unfit, non-acclimatized individuals is high”; 27.9–30.0°C “cancel level for exertional heat stroke risk”; 30.1–32.2°C “cancel or stop practice and competition”; $\geq 32.3^\circ\text{C}$ “Cancel exercise” [62,63].

Large-scale teleconnection pattern

Wakabayashi and Kawamura [22] identified the upper- and mid-air dynamics that influence summer extremes in Japan. They also found that August in eastern Japan had the highest positive correlation with the PJI, a near-surface (850hPa flow), and some association with the WJ, which is measured at the 200hPa level (approximate level

of commercial air flights). The WJI and PJI were calculated in the current analysis as follows:

$$PJI = \frac{[Z_{850}^*(155^\circ E, 35^\circ N) - Z_{850}^*(125^\circ E, 22.5^\circ N)]}{2} \quad (2)$$

where, Z is the geopotential height shown in subscript (i.e. 200hPa and 850hPa for WJI and PJI, respectively) at the geo-locations given in parenthesis. Z is a height calculation (m) that factors in the gravitational pull on a fluid layer. Changes in fluid density (which are tied to temperature), for example, can alter how gravity pulls on the layer and therefore its height above sea-surface.

Principal Components Analysis (PCA) & WGBT quartiles

We conducted a PCA as a dimension-reduction method, using an orthogonal transformation, to convert our set of correlated predictor variables of August daytime WGBT into a set of linearly uncorrelated principal components (PCs). Our predictor variables were: (1) local meteorology (namely solar radiation, moisture, and winds combined as the WGBT variable)²; (2) NINO3 and (3) NINO3.4 anomalies; (4) PJI and (5) WJI. The PCA method essentially allows us to determine (or “tease out”) which of the five predictor variables, and at what time of year (e.g. previous MAM), are playing the main role in causing a higher or lower mean daytime August WGBT value in Tokyo. Thus, we also looked at these variables within four seasons (based on traditional ENSO season parameterizations): September, October, November (SON of previous year), December, January, February (DJF, 1-month previous year, 2-month current year), MAM, and JJA, as shown in [Figure 2](#). The final simple PCA matrix was five predictive meteorological variables \times four ENSO seasons across 36 years, and was used to create the uncorrelated PCs to predict August mean daytime WGBT. Given the dynamic feedback between our variables (for example, the SSTs for NINO3 and NINO3.4 can be highly correlated due to their close geophysical proximity), the use of PCA allows us to understand and scale the individual forcings from each (see also Richman [64] Figure 9). In summary, our matrix was designed to study the effect of ENSO

season on regional and local atmospheric dynamic, over 36 years, which is an appropriate range that would give us a climate signal.

As we are looking for lead-time awareness, we eliminated the August WGBT 1980 datum from our calculation to initiate the sequencing such that SON ENSO 1980 data were analyzed as a potential forcing potential on August 1981 WGBT values, and so on, for the subsequent years. PJI and WJI values by ENSO season were also analyzed and used ± 0.50 as the PCA cutoff value. From the output correlation covariance matrix, coefficient (eigenvalues) of 1 were retained in our unrotated matrix, representing PCs that explained 80% of the total variance. Given that the variance explained was so high, we did not rotate the matrix. We then more deeply analyzed the variables that explained $\sim 90\%$ of the variance within each component.

Finally, we calculated the quartile indices of the local WGBT, binning the values in the 25th, 50th, 75th, and 100th percentiles. We ran two-tailed t-tests to determine the significance between the means of each quartile and determine partition thresholds. Each quartile was then qualitatively assessed alongside historical ENSO data from the JMA and NOAA/NCEP Climate Prediction Center [44] to ascribe the ENSO phase, duration in phase, and intensity for NINO3 and NINO3.4, respectively, by WGBT quartile. This method was conducted to better understand the other characteristics of ENSO that the PCA may be identifying.

Intraurban heat mapping

To further explore and demonstrate finer-scale variability in urban heat exposures, we utilize the 24 weather stations noted above (2008–2018 inclusive). It is important to note that 10 years of data is a relatively short period given a climate time scale; however, AWS data are limited to this time frame. These data and related analyses are not connected to the large-scale analysis.

From the AWS data, we created continuous spatial surfaces at a 500 m resolution for daytime air temperatures (0500 h–1900 h) using random forests-based regression kriging (RFRK), essentially “filling in” gaps where stations are not present using related land-use

information [65,66]. The RFRK integrates five environmental variables that were found to significantly correlate with T_a from the 24 stations. These variables include normalized difference vegetation index (NDVI), brightness of nighttime lights (NTL), land elevation, and land surface temperature (T_{sfc}), as well as station-based RH. Each are described below:

- (1) The 16-day NDVI (MOD13A1) images collected in August during 2008 and 2018 were obtained from the U.S. Geological Survey (USGS) [67] at a 500 m spatial resolution. These images were aggregated into one image to show the average NDVI during the study period.
- (2) Brightness of NTL data were retrieved from the monthly VIIRS-DNB³ product at a 500 m resolution from the NOAA Centers for Environmental Information [68]. Land surface temperature taken by MODIS⁴ has been widely employed to predict T_a [69], and so was adopted as a predictor in the RFRK model.
- (3) The 8-day land surface temperature (MOD11A2) products taken in August during 2008–2018 at 1 km spatial resolution were retrieved from USGS [67] and combined into one image to represent the mean land surface temperature.
- (4) Digital elevation was used as an estimator to account for the impact of terrain features on T_a . These data were obtained from the Global Land 1 km Base Elevation digital elevation model.

All satellite images were resampled to the same spatial resolution (i.e. 500 m) through a bilinear approach [66] and further applied to the RFRK model to produce the spatial surfaces for T_a . Detailed information on the RFRK method can be referred to elsewhere [65,66,70]. The brightness of NTL and NDVI have proven to be good proxies for anthropogenic activity, which has a large impact on T_a in urban areas [71]. The daytime (0500–1900 hr) and midday (1200–1500 hr) average and maximum T_a were calculated for the location of each venue, with daytime values aligning with MERRA-2 data used (and daylight hours),

and midday hours similar to Gerrett et al. [9] who found this period to be the hottest time of day during the Olympics.

Results

Regional long-term WBGT levels

General regional WBGT data from MERRA-2 calculations display daytime average values ranging from 25.8°C to 29.1°C in Tokyo in August between 1980 and 2016, where the highest daytime *mean* WBGT (29.1°C) was in 1996. The 35-year average daytime WBGT in August was 27.0°C between 1980 and 2016. More recently, daytime WBGT values in August for 2012–2014 were in the highest quartile (28.43–29.12°C), with 2015 and 2016 in the second-highest quartile (27.86–28.19°C) (these data are presented within Table 6).

Large-scale (Planetary) results: Principal Components Analysis (PCA)

Tables 3 and 4 provide PCA coefficient and loadings, respectively. Overall, the ENSO seasons DJF (*coefficient: 2.1870*) and JJA (*coefficient 2.1718*) carry slightly higher coefficients over the transitional seasons. The findings support a particular seasonal excitation of the Rossby wave, which is a planetary wave that can influence regional circulations [40], such as the PJO [21,22,33] and the WJ [39].

Five PCs were identified, capturing the planetary, regional, and local meteorology (WBGT as an index of solar, moisture, and wind combined) impacts on mean daytime WBGT in August in

Table 3. Principal component evaluation (PCA) of each ENSO season. Higher coefficients indicate a stronger relationship between the WBGT levels in August and the seasonal lead time (previous season; e.g. previous December, January, February (DJF) or June, Jun, August (JJA), etc.). Lead times of DJF and JJA have the strongest relationship, indicating possible planetary wave excitation in those seasons as a result of the air–sea interactions in the ENSO region. It is possible that the slightly higher coefficient scores are indicating Rossby wave excitation, and that such activation is strongest in DJF with another pulse in JJA.

SON (season 1) coefficient	DJF (season 2) coefficient	MAM (season 3) coefficient	JJA (season 4) coefficient
2.0939	2.1870	2.0721	2.1718

Table 4. Principal component analysis (PCA) loading scores (by ENSO season) indicate which variables play a main predictive role for daytime average August WGBT levels and in which season. Given that mid-latitude atmospheric systems are inherently non-linear, and given the high auto-correlation between our variables (e.g. ENSO can give rise to PJI features [21], we used ± 0.50 as the PC cutoff value). Recall that for predicting the levels in August, SON and DJF loadings are for the previous year, and MAM and JJA are for same year (see Figure 2).

Meteorological Season	Variables	PC1	PC2	PC3	PC4	PC5
September-October-November (SON)	var1 (NINO3)	0.650	-0.245	-0.093	0.095	0.707
	var2 (NINO3.4)	0.637	-0.285	-0.127	0.018	-0.705
	var3 (PJI)	0.213	0.698	-0.088	0.676	-0.056
	var4 (WJI)	-0.342	-0.596	-0.208	0.695	-0.013
	var5 (local meteorology) ^a	0.092	-0.127	0.961	0.223	-0.032
December-January-February (DJF)	var1 (NINO3)	0.600	0.365	0.020	-0.055	0.709
	var2 (NINO3.4)	0.579	0.414	0.013	0.015	-0.702
	var3 (PJI)	-0.371	0.592	0.105	0.706	0.060
	var4 (WJI)	0.390	-0.543	-0.257	0.698	0.011
	var5 (local meteorology)	0.125	-0.223	0.960	0.111	-0.009
March-April-May (MAM)	var1 (NINO3)	0.645	0.191	0.166	-0.064	0.718
	var2 (NINO3.4)	0.624	0.236	0.229	-0.161	-0.691
	var3 (PJI)	-0.176	0.666	0.236	0.686	-0.013
	var4 (WJI)	0.398	-0.477	-0.364	0.689	-0.085
	var5 (local meteorology)	-0.075	-0.487	0.855	0.160	0.013
June, July, August (JJA)	var1 (NINO3)	0.615	0.192	-0.283	0.141	-0.697
	var2 (NINO3.4)	0.617	0.224	-0.259	-0.010	0.709
	var3 (PJI)	0.178	0.401	0.807	0.396	0.019
	var4 (WJI)	-0.205	0.761	-0.032	-0.609	-0.082
	var5 (local meteorology)	-0.410	0.417	-0.449	0.672	0.071

^aSolar, moisture, winds, temperature combined for previous ENSO season WGBT.

Tokyo. The physical explanation of these findings are as follows, from the most important (PC1) to least important (PC5):

PC1: All ENSO seasons loaded NINO3 and NINO3.4 into PC1, indicating that air–sea interactions in this Pacific region (see Figure 1) for all seasons are a significant contributor to August WGBT in Tokyo.

PC2: Both regional circulations (WJ and PJO) loaded on PC2, but differently across seasons. Positive PJO and negative WJ appeared in SON and DJF (and almost MAM), while only WJ in MAM and JJA. These findings make physical sense as the WJ does not have a signal (and is thus not connected to August Tokyo WGBT) Oct–Feb, whereas the PJO is significantly connected to WGBT at this lead time.

PC3: Seasonal differences loaded onto PC3. Here, local meteorology was a significant forcing for SON, DJF, and MAM, but the PJO loaded here for JJA. While further analysis is needed, we believe that the change in loading of local meteorology in JJA (versus the other ENSO seasons) is indicative of a change in fronts that is different from the others (e.g. a seasonal frontal system, called the Baiu front, moves in early summer and is then displaced by BOH development in August that brings high pressure and clearer skies).

PC4: The regional circulations appear again, yet differently across seasons. The PJO/WJ loaded in PC4 in SON, DJF, and MAM. Conversely, a negative WJ and local solar/moisture loaded for JJA.⁵

PC5: While PC5 represents lower importance to explaining August WGBT values, it is critical to note that a positive NINO3 state in SON, DJF, and MAM bears more correlation than NINO3.4, which has a negative relationship in these seasons. However, NINO3.4 in JJA has a higher correlation with August WGBT compared with NINO3 in that season.

Table 5 presents the variance explained by each PC. Each ENSO season captured a total of 99.9–100% of the variance in daytime August WGBT, which is an indicator that the most relevant and pertinent flows for Tokyo weather were captured, and that each ENSO season and NINO3/NINO3.4 regions have variable forcings on Tokyo's August WGBT values.

The three most important variables are NINO3, NINO3.4 (NINO3/NINO3.4), which together explain about 70% for each season; adding the PJO bring the strength to 90%. Specifically:

- **NINO3** was the most significant variable for all seasons, explaining slightly more variance

Table 5. Percent variance explained by each of the five PC variables in predicting the mean daytime WBGT in August within each ENSO season. Notable findings are bolded, and variables are ranked from highest explanatory power to lowest with 99–100% variance explained by our variables, we reasonably determine that the pertinent variables for Tokyo’s mean daytime WBGT in August are isolated, with NINO3, NINO3.4 and PJ being the most important. Note that DJF and JJA explain the most variance in NINO3, whereas NINO3.4 is a greater factor in MAM. Overall, however, NINO3 is the dominant forcing on Tokyo WBGT, which is consistent with other findings (e.g. Urabe and Maeda [34]). MAM is the only season with a relevant coupling with NINO3.4. The PJ is a significant factor in SON and JJA, indicating the dominance of the PJ (a largely summer/late summer circulation from Tokyo’s south) on WBGT levels. DJF: December-January-February; MAM: March-April-May; JJA: June-July-August; SON: September-October-November.

Variable	Prior season to August			
	SON	DJF	MAM	JJA
NINO3	41.88	43.74	41.45	43.33
NINO3.4	29.76	29.41	30.69	25.29
PJ	20.33	19.26	16.80	20.13
WJ	7.52	6.99	8.90	9.40
Local meteorology ^a	0.51	0.59	2.20	1.74
Total variance	100%	99.99%	100%	99.89%

^aSolar, moisture, winds, temperature combined for previous ENSO season WBGT.

in DJF (43.74%) and JJA (43.33%) than in SON (41.88%) or MAM (41.45%)

- **NINO3.4** was the second most significant region of influence in MAM (30.69%), followed closely by SON (29.76%) and DJF (29.41%).
- **PJ** was most prominent in SON (20.33%) and JJA (20.13%), indicating the dominance of the PJ (a largely summer/late summer circulation from Tokyo’s south) on WBGT levels. Its relatively high value (19.26%) in DJF (which is “off-season” for the PJO) may indicate Rossby wave excitation that affects flows in the PJO region of the Pacific tropics.
- The remaining artifacts (WJ and local meteorology) are more situational. They are less effective in explaining WBGT levels in August in Tokyo, the latter owing to solar and moisture being a byproduct of the larger planetary/regional circulations and subsequent frontal systems that change in summer.

WBGT quartiles: Results & qualitative analysis

Through segmenting the MERRA-2 WBGT data by quartile (Q) (see Table 6), we investigated the commonalities among our variables that seem to

describe the given quartiles, where Q1 represents the lowest mean daytime WBGT in Tokyo in August, and Q4 the highest. All mean WBGT values are significantly different from each other ($p < 0.05$), and thus the mean WBGT in each quartile is distinct, which is a key indicator that separate atmospheric processes likely explain the resulting WBGT values in Tokyo.

Q1 and Q2 (coolest) are both El Niño-centric (with four and six events, respectively), and both had two La Niña events each. However, Q1 is linked to more neutral phases (four) versus Q2 (one). Q1 and Q2 had six Asian/Indian Monsoon events, whereas Q3 and Q4 each had one monsoon event, respectively. Further, Q3 and Q4 (warmest) both show a La Niña dominant pattern (with four and five events, respectively), and had a similar number of “neutral” events (two and three, respectively) and El Niño events (two and one, respectively).

The largest distinction between Q3 and Q4 is in the duration of the ENSO phase in both NINO3/3.4, especially for the La Niña events. In Q3, NINO3.4 enters a La Niña phase earlier (~1.5 months) than NINO3. In Q4, NINO3 exhibits a La Niña phase for 11.5 months, again ~1.5 months earlier than NINO3.4. While the PCA identified temporal (e.g. ENSO season) and spatial (ENSO, PJO, or WJ) domains, the quartile analysis added critical context on the type, or “flavor” of ENSO identified by the PCA.

As each WBGT quartile contained a “neutral” phase (currently predicted for 2020) we explored the solar and moisture tendencies of each of the 11 neutral events. Using monthly averaged daytime (0500–1900 hr) solar radiation, RH, and dew point temperature—for our period of record—we found that solar radiation was most intense in Q3 and Q4 (highest WBGT values) during neutral events (five total between Q3 and Q4), with lower moisture profiles. This finding indicates that increases in radiation dominate discomfort at the highest WBGT in Tokyo during an ENSO neutral year, which is most probable in August 2020 [37]. Conversely, during neutral years in Q1 (five events), moisture levels dominated relative to Q4.

Overall, the PCA and quartile analysis indicate the following in predicting mean daytime WBGT levels in Tokyo in August:

Table 6. MERRA-2 August WBGT data (mean daytime 0500–1900 hr) segmented by quartile using data from 1981 to 2016, inclusive. P-values show the significant difference between the two quartiles ($Q_n - Q_{n-1}$) and indicate that distinct atmospheric processes explain the mean August WBGT values. Commonalities among the variables within each quartile are also presented. SST: sea-surface temperature.

Quartile	Mean daytime WBGT August average (°C) (range)	p-value to next nearest neighbor	Atmospheric commonalities, salient features, and number of ENSO phase events within quartiles between 1981 and 2016
Q1 (lowest WBGT)	26.6°C (25.71–27.19)	Q1–Q2: P = 0.00005	<ul style="list-style-type: none"> • Described by El Niño or neutral years and West-Asian Jet presence (e.g. influence of Indian Monsoon^b) • 10 events: four El Niño (4), five neutral (5), one (1) transition from El Niño to La Niña.
Q2 ^a	27.6°C (27.21–27.86)	Q2–Q3: p = 0.0001	<ul style="list-style-type: none"> • El Niño phase, with very strong/strong El Niño SST development in DJF in NINO3.4 • Largest standard deviation in NINO3 SST, and top-ranked DJF SST values for same region in Pacific; hence, showing interplay between regional dynamics. • 9 events: six strong/very strong El Niño (6), two La Niña (2), and one neutral (1).
Q3	28.1°C (27.86–28.19)	Q3–Q4: p = 0.00006	<ul style="list-style-type: none"> • La Niña phase with similar phasing, but slightly different timings in both NINO3 (avg 8.3 months) and NINO3.4 (9.8 months) • Strongest NINO3.4 SST in NDJ (not DJF), low PJI (indicates some decoupling/weakening of baroclinic-barotropic transition), and some La Niña development (cooler SST). • 8 events: four La Niña (4), two El Niño (2), two neutral (2).
Q4 (highest WBGT)	28.6°C (28.43–29.12)	-	<ul style="list-style-type: none"> • Significant La Niña pattern (cooler SST) in both NINO3 and 3.4^c; similarities in phasing, near same duration of phase and intensities in both NINO3 (avg 11.5 months) and 3.4 regions (10 months).^c • Lowest PJI values for all quartiles. • Hottest August WBGT (in 1996) is associated with most negative WJI of all quartiles, which was a “neutral” year that followed a moderate La Niña, thus possibly still subscribing a La Niña influence on high August WBGT levels in Tokyo. • 9 events: five La Niña (5), three neutral (3), one El Niño (1).

^aQ2 exhibited the highest number of “strongest El Niño” events in NINO3.4 for DJF season, indicating that SST in DJF of the preceding/early year has an influence on August WBGT in Tokyo. This finding further implies that NINO3 and NINO3.4 phases and intensities are predictive factors, also underscoring (or reaffirming) the findings of the PCA.

^bSee Supplemental Material.

^cThe La Niña intensities are the greatest contrast to the La Niña patterns in Q3.

- Low WGBT values are associated with a neutral or El Niño phase.
- Moderate WGBT values are associated with a neutral or El Niño phase.
- High WGBT values are most influenced by La Niña, and both NINO3 and NINO3.4 regions, but NINO3 is noticeably a stronger influence for Tokyo.
- The highest WGBT values exhibit the strongest La Niña features and longer duration in that phase for **both** NINO3 and NINO3.4 regions.

Pacific-Japan oscillation analysis

An analysis of the PJI by ENSO season and WGBT quartile was conducted to identify the features of the PJO in SON, DJF, and JJA that can explain August WGBT in Tokyo. Total ENSO season median PJI was calculated and used to discretize PJI by WGBT quartile. We found a pattern in SON and JJA where PJI quartiles (Pq) could explain cool/warm WGBT in ENSO neutral and El Niño phases for SON and neutral for JJA. A La Niña phase, it should be noted, showed zero pattern consistency in each ENSO season. This finding is shown in graphical form and further examined in the Supplemental Material. We do, however, see a periodic pattern of the PJI within each WGBT quartile when the data are grouped by neutral, El Niño, and La Niña.

Intraurban heat variability

Figures 4 and 5 display the air temperature variability across Tokyo prefecture in August (Sapporo not shown) using the RFRK method. Results focus on the daytime (0500–1900 hr) and midday (1200–1500 hr) periods, showing the mean daytime T_a (\bar{T}_a) across 10 years, as well as the average daytime high temperature (\bar{T}_{max}). While slight variation is seen across the city, most venues are not located in the absolute hottest location (based on daytime \bar{T}_a), and minimal variation overall is present ($<1.2^\circ\text{C}$ and 1.7°C difference for mean T_a and \bar{T}_{max} , respectively). The mean daytime and midday T_a across all outdoor venues average 28.7°C (range 0.6°C) and 30.6°C (range 0.7°C). Similarly, the respective T_{max} have minimal

variability between venues [31.1°C (range 0.6°C), versus 31.2°C (range 0.7°C)]. The similarity of the latter \bar{T}_{max} between daily and midday indicate that the highest T_a at the venues occurs between 1200 and 1500 hr. Hourly August averages and ranges for each station can be seen in Figure 6.

Importantly, these daytime \bar{T}_a indicate very hot conditions expected based on a 10-year station climatology, with little variation expected between the venues given the conservative nature of changing T_a [72], the long-term averaging used, and standardized siting of AWSs. Most urban heat studies utilize T_{sfc} to show intraurban temperature variation, which has much less relevance for a human's thermal experience in a city compared to solar radiation, wind, or humidity [73]. However, T_{sfc} is more accessible data (via remote sensing) and can be changed through design (e.g. surface type, color, and shading; building orientation), as shown by Vanos et al. [16] for the previous marathon course. Further, although shading provides reprieve from the sun and lower T_{sfc} , athletes will not be competing in the shade (yet shading will be an important factor to protect volunteers, workers, and spectators).

In comparing the venue \bar{T}_a , Tokyo Stadium (football, rugby, modern pentathlon), Olympic Stadium (athletics, football), Oi Hockey Stadium (hockey), and Saitama Stadium (football) display the highest daytime \bar{T}_{max} and \bar{T}_a over the last 10 years ($\bar{T}_{max} \sim 31.3^\circ\text{C}$ and $\bar{T}_a \sim 28.8^\circ\text{C}$); however, as stated, minor differences are present in the averages between all venues). Venues located on or near the ocean show a slightly lower \bar{T}_a , yet still average $>30^\circ\text{C}$ midday \bar{T}_a and \bar{T}_{max} . Sapporo shows significantly lower T_a , with a 10-year daytime average of 23.6°C based on the AWS, reaching a \bar{T}_{max} of 26.3°C . For full results interpolated by venue, see Table 7.

Although T_a is an important indicator of heat stress, the event timing and length will likely be more important for EHI and HRI protection and planning (particularly given the overall similarities between the \bar{T}_a across venues). Tables 8 and 9 display the events that have a large percentage of time during the hottest portion of the day (midday) and event duration. Road cycling

Table 7. Average and maximum air temperatures in Tokyo daytime (0500–1900 hr) and midday (1200–1500 hr) at each venue, for the month of August (2008–2018). These weather stations are not located at venues; the data presented here are based on RFRK-produced data for spatial interpolation (shown in [Figures 4](#) and [5](#) maps). Further, some venues are outside the region (e.g. mountain biking) and could not be included in the RFRK; thus, only venues within the Tokyo region are listed. SD: standard deviation.

Sport	Venue no.	Mean daytime T_a (°C)	Maximum	Minimum daytime T_a (°C)	Mean midday T_a (°C)	Maximum midday	Minimum midday T_a (°C)
			daytime T_a (°C)			Maximum midday T_a (°C)	
Archery	2	29.0	31.5	25.2	30.9	31.6	30.4
Football	13d	28.8	31.4	25.1	30.9	31.5	30.1
Aquatics	1	28.7	30.9	25.6	30.3	30.9	30.2
Athletics	3	28.8	31.3	25.3	30.8	31.5	30.1
Canoe & Kayak	7/8	28.8	31.1	25.5	30.6	31.2	30.2
Cycling (BMX)	9	28.7	30.9	25.6	30.3	30.9	30.2
Equestrian	12	28.6	31.0	25.3	30.5	31.1	30.2
Football	13a	28.7	31.3	24.9	30.8	31.5	30.0
Football	13e	28.7	31.2	25.2	30.6	31.3	29.9
Football	13 f	28.8	31.3	25.3	30.8	31.5	30.0
Golf	14	28.6	31.1	24.8	30.6	31.3	29.9
Hockey	15	28.8	31.3	25.4	30.7	31.4	30.1
Mod. Pentathlon	16	28.7	31.3	24.9	30.8	31.5	29.9
Rowing	17	28.6	31.0	25.3	30.5	31.1	30.0
Rugby	18	28.7	31.3	24.9	30.8	31.5	29.9
Shooting	20	28.6	31.1	24.9	30.6	31.3	29.9
Skateboarding	21	28.7	30.9	25.6	30.3	30.9	30.2
Tennis	23	28.8	31.2	25.4	30.6	31.3	30.2
Triathlon	24	28.7	30.9	25.6	30.3	30.9	30.2
Beach Volleyball	25	28.7	30.9	25.6	30.3	30.9	30.2
Football 5-a-side	26	28.7	30.9	25.6	30.3	30.9	30.1
Baseball/Softball	6	28.8	31.2	25.3	30.7	31.4	30.0
Sailing	19	28.7	30.9	25.6	30.3	30.9	30.1
Average \pm SD (°C)		28.7 \pm 0.08	31.1 \pm 0.17	25.3 \pm 0.26	30.6 \pm 0.20	31.2 \pm 0.20	30.1 \pm 0.12
Range (°C)		0.4	0.6	0.6	0.6	0.7	0.6
Race Walk & Marathon	4 & 5	23.6	26.3	20.1	24.7	26.1	24.7

has ~45% of its events midday and is also the longest event, with athletes at high metabolic intensity throughout. Similarly, baseball and softball are long events with a high proportion of competition midday (43% and 37%, respectively), yet have lower intensities and will be closer to a location where athletes can seek cooling and supplies.

Alternatively, sailing has the highest proportion of their given competition hours midday (48%), yet the length of competition is much shorter, and the midday \bar{T}_{max} is slightly lower due to being near or on the water. Finally, golf also depicts a high-risk situation based on event length (4–5 h) and timing (37% midday) yet has a lower metabolic intensity.

Almost all outdoor Paralympic sports will occur during some portion of midday; however, the events of greater concern are wheelchair tennis and road cycling that take longer to complete, are intense, and are held midday for 35% and 38% of the planned competition time for each

respective sport. In general, each event will require unique heat-preparedness plans, but certain events will be at a higher risk given the location, timing, length, and intensity.

Discussion

Physical explanations: combining the PCA, variance, quartile, and PJI analysis

We used stochastic methods (random probability) to identify patterns of probabilities and patterns of ENSO with mean daytime WGBT levels in Tokyo for August across 36 years. The PCA identified important spatial domains (NINO3 and NINO3.4) that give rise to regional circulation (i.e. PJO); together, the three predictors explain ~90% variance in August daytime WGBT in Tokyo in the 36-year period. Further, SST in winter (DJF) and height of the 850hPa atmospheric layer (PJ) in SON appear to be the relevant temporal scales to observe potential setup of patterns to better predict August WGBT range.

Table 8. Outdoor Olympic events ordered by percentage of time between the hours of 12:00–3:00 pm, aligned with the average length of the given race, event, match. A deeper red color paired with darker blue indicates a long event occurring at the hottest time of the day, and thus higher risk. See Figure 2 for venue locations and Table 2 for names.

Venue No.	Sport	Total event hours scheduled between 12pm–3pm (hh:mm:ss)*	% event hours between 12pm–3pm*	Average Length of Match, Race, or Event (minutes)*
19	Sailing	28:00:00	48%	65
11	Cycling Road	8:00:00	45%	400
6	Baseball	21:00:00	43%	210
7	Canoe Slalom	8:00:00	42%	10
20	Shooting Clay	14:45:00	41%	25
21	Skateboarding Street	3:50:00	39%	10
20	Shooting	20:00:00	39%	25
6	Softball	17:00:00	37%	210
14	Golf	24:00:00	37%	270
21	Skateboarding Park	3:20:00	36%	10
23	Tennis	204:00:00	34%	180
22	Surfing	10:00:00	30%	40
8	Canoe Kayak Sprint	4:50:00	25%	10
3	Decathlon & Heptathlon	3:25:00	22%	60
15	Hockey	28:30:00	20%	60
16	Modern Pentathlon	3:00:00	16%	25
2	Archery	8:05:00	16%	60
9	Cycling BMX	1:05:00	12%	15
25	Beach Volleyball	8:40:00	8%	60
3	Athletics - Field	9:10:00	9%	120
3	Athletics - Track	4:30:00	8%	20
17	Rowing	0:40:00	3%	25
13a-f	Football	2:00:00	1%	105
10	Cycling Mountain Bike	0:00:00	0%	120
12	Equestrian	0:00:00	0%	225
5	Marathon	0:00:00	0%	150
1	Marathon swimming	0:00:00	0%	15
4	Race walk	0:00:00	0%	25
18	Rugby	0:00:00	0%	80
24	Triathlon	0:00:00	0%	120

*Based on men and women combined.

NINO3 was significant in all seasons for influencing Tokyo, a finding that is consistent with Urabe and Maeda [34]. DJF and JJA NINO3 and NINO3.4 are the most significant temporal domains when this teleconnection bears a stronger influence.

Further, each season may be showing a particular Rossby wave excitation that is relevant [40] to August WBGTs in Tokyo. This excitation likely leads to the PJ activity, which was clearly identified as the dominant regional flow (compared with

Table 9. Outdoor Paralympic events ordered by percentage of events between the hours of 12:00–3:00 pm. Higher red color paired with darker blue indicates a long event at the hottest time of the day.

Venue	Sport	Total event hours (hh:mm:ss)*	Total event hours between 12pm–3pm (hh:mm:ss)*	% event hours between 12pm–3pm	Average Length of Match, Race, or Event (minutes)*
20	Shooting	43:45:00	18:15:00	42%	25
9	Road Cycling	31:35:00	12:00:00	38%	120
23	Wheelchair Tennis	435:00:00	153:00:00	35%	180
2	Archery	62:35:00	13:35:00	22%	60
3	Athletics	55:30:00	8:30:00	15%	45
25	Football 5-a-side	31:35:00	4:00:00	13%	40
17	Rowing	32:45:00	3:40:00	11%	30
24	Triathlon	10:00:00	1:00:00	10%	120
8	Canoe	7:50:00	0:40:00	9%	10
4	Marathon	4:30:00	0	0%	120
12	Equestrian	5:20:00	0	0%	225

*Based on men and women combined.

WJ), supported by Wakabayashi and Kawamura [22] for eastern Japan. The PJO may also be a self-sustaining flow during the Asian/Indian monsoon [74], which is a significant regional flow pattern largely from the south into Tokyo (outlined in Supplemental Material).

Confirming a teleconnection pattern, however, will require model runs of planetary to regional dynamics [75]. Yet both the coolest average August WGBT (1981) and the warmest (1996) occurred in “neutral” ENSO years, with an active Indian Monsoon. Further, given the “many flavors of ENSO” (*personal communication*, Dr. Kevin Trenberth), we can at best observe past ENSO behavior in the 1990s to lead to different teleconnection outcomes [26].

Quartile analysis identified ENSO phase, duration, and intensity. A neutral phase—currently expected for this summer—occurred across all WGBT quartiles. La Niña was the dominant pattern in the two warmer WGBT quartiles (Q3, Q4). This finding, when combined with the JJA strength and activity of the PJ, supports similar findings [21,22,33]. Conversely, a dominant El Niño and neutral phase were noted in the cooler WGBT quartiles (Q1, Q2), also linked to higher

moisture levels and favored precipitation. The highest WGBT (Q4) events had the highest solar intensity and may have more of a BOH influence, as high-pressure systems reduce convection and cloud cover (increasing radiation levels).

Finally, median and quartile analysis of the monthly averaged PJI shows some early promise that the PJI can be a predictor in neutral and El Niño years in SON and JJA, in particular. Moreover, 35°N latitude has more forcing on the PJO, and that La Niña years show more spread/variability in the PJO. It should be noted that our dataset of 35 years was too small to transform the data, and that the data used were aggregate August WGBT values. Higher temporal resolution analysis of the PJ is encouraged for all phases, but especially for La Niña years, to resolve its factors of influence on local WGBT values for the Games and perhaps future events.

Lead times from these results, particularly connections of DJF and MAM with Tokyo August WGBT, offers valuable advanced information for anomalous heat preparedness for Tokyo 2020. ENSO-neutral conditions are expected to continue through spring 2020 (65% chance), which is when

the next ENSO season will be more predictable (see Figure 2). Further, results here are for average conditions, and finer temporal resolutions, such as how the BOH (increase heat and humidity) influences Tokyo on a 7–10 day scale [3]. Future applications of such climatological risk assessments could be improved through a probability analysis and using a larger number of grid cells for an aggregate value as inputs, as meteorological drivers will be from other geographical sources. Second, attempting daily versus monthly WBGT daytime levels could also lend itself well to more precise planning.

Intraurban temperature, WBGT, and heat vulnerabilities

Intraurban T_a variations in August across a 10-year climatology indicate routinely hot conditions with high \bar{T}_{max} and \bar{T}_a , yet minimal variability across the city. Although urban design within Tokyo can affect experienced thermal and radiative conditions [12,16], these differences are largely due to shading or wind. The athletes will almost always be in the sun during daytime competition, and wind will vary greatly by venue type and/or orientation. These microclimate parameters of wind (for evaporative cooling) and solar radiation (radiant heating) are more easily altered through design as opposed to T_a [72].

Tokyo's climatology and our analyses indicate that all outdoor venues will be hot and humid, increasing EHI and HRI risk, with the larger-scale teleconnection patterns potentially playing a larger role in determining just how oppressive the conditions will be. Athletes will be at risk, and given that weather cannot be changed (extrinsic and non-modifiable), heat preparedness efforts should focus on modifiable and intrinsic personal factors (e.g. acclimation, hydration, nutrition, pre-cooling), as well as allowing breaks when needed and lowering temperatures in warmup areas (see Figure 1 in Hosokawa et al. [61]) Enhanced focus can be given to longer and more intense events, and those further from cooling relief areas (e.g. road cycling and mountain biking).

This study applied long-term data from 24 weather stations across Tokyo applying novel interpolation mapping to minimize scalar

incongruence in decisions for heat preparedness [76]. Gerrett et al. [9] utilized a single weather station for Tokyo ward and the same WBGT model [52] used here, and similarly showed the WBGT to vary by 4°C between the early morning and the early afternoon, with maximum values between noon and 3 pm. The current schedules for outdoor events avoid competitions during this time insofar as possible (Tables 8 and 9); however, spectators and volunteers preparing for the mid-day events (1200–1500 hr) will likely be in the periphery of the venue, waiting to enter the gated venue (spectators) or organizing traffic and providing services outdoors (volunteers) for many hours combined.

Athletes who have shorter events (e.g. sprint events, archery) are also at a lower risk for sunburn (and potentially heat illness) versus longer events (e.g. women's tennis, golf, cycling, marathon) [77,78]. Research shows that many athletes may not use sunscreen due to concerns about performance, thermal or physical discomfort, or impacts on perspiration [79,80]; however, sunburned skin also reduces one's ability to thermoregulate [80,81].

Within the Paralympic Games, athletes competing with an SCI experience a loss of sweating capacity and vasomotor control below the lesion level of their injury [82–84], thus impacting the ability to thermoregulate [85]. Veltmeijer et al. [86] empirically showed that core temperatures rose more in wheelchair tennis players with CPI compared to able-bodied players. A loss of surface area (when seated) for sweating and convective heat losses also increases body heat storage in wheelchair athletes. Athletes with an SCI are eligible to compete in 18 sports, yet heat-health polices exist merely for wheelchair tennis athletes [87].

Athletes with CP have both physiological and cognitive challenges. Physiologically, movement efficiency is decreased; thus, there is a greater heat production for a given external workload in those with CP, elevating thermal strain [88]. Cognitively, those with CP have more difficulty with pace awareness, environmental interpretation, thermal state, and perceived effort, and thus may experience higher incidence EHI due to not downregulating their effort as thermal strain rises [88,89]. Athletes with MS experience thermoregulatory dysfunction

due to lesions in the central nervous system (specifically the hypothalamus) that may impair thermoregulatory function [90].

Heat-preparedness efforts

Notable heat precautions were made in past host cities in warm climates, such as Atlanta and Los Angeles, for dealing with the high heat. For example, approximately 645,000 cups of water, 600,000 hats, and 395,000 packets of sunscreen were used in the city of Atlanta at heat-related illness prevention stations, which were strategically placed in areas with high pedestrian traffic and allowed for on-site management of mild heat-related symptoms [19]. This effort helped to limit the heat-related response emergencies to 2% of the calls in 1996. For athletes, there should be a large emphasis on heat acclimation [9], particularly since pre-cooling opportunities are limited in most sports [91]. Due to the shifting Tokyo summer conditions between July and August (to hotter and more humid), athletes entering the Olympics Games who compete earlier in the schedule should focus on forced heat acclimation as natural acclimatization is unlikely to occur [9]. Those in the Paralympic games should have sufficient time to acclimatize. All athletes and attendees of the Games should recognize that they are not exempt from HRI in Tokyo's normal conditions, even when the environmental conditions may be relatively moderate.

Important considerations

This work is the first multi-scalar interdisciplinary study to examine WBGT and T_a in relation to ocean-atmosphere teleconnections combined with local temperature extremes, respectively. We focus our communication toward a broad community of researchers and practitioners and attempt to communicate complex, yet relevant, information on an important and timely societal topic.

Our application of atmospheric and biometeorological sciences to specific applied health applications and societal benefit has further identified new research and modeling efforts, and underlines the complexities of working across data types, scales, and disciplines. For example, since we

downscaled to Tokyo metropolis, “noise” in the analysis became an issue, and thus the WBGT models were created for daytime values across the month of August (hence, characterization of monthly average daytime WBGT), and caution is advised to not imply that all August days in 2020 will behave as the “average” on individual days or weeks. Actual individual days could fall *at, above, or below* any quartile range during a synoptic period (~7–10 days). Further, while we have derived overarching tendencies for August WBGT starting in DJF (2019/2020), a different type of analysis will be needed as we approach August to observe the evolving regional dynamics on a climatological-to-meteorological scale to improve decision-making.

Concluding remarks

Holding the 2020 Olympic and Paralympic Games in late summer in the subtropical climate of Tokyo, Japan favors heat stress concerns and issues for spectators, athletes, and workforce. Planetary atmospheric linkages that emanate from the ENSO region influence temperature, moisture, and radiation regimes in Tokyo in August (and thus WBGT levels). Findings herein may inform the preparedness of the IOC, the Organizing Committee of the Olympic Games (OCOG), as well as those attending or competing at the Games or future late summer events in Tokyo. While it is certain that August will be hot and humid, our methods and findings show the potential added precision value (as in “*how much hotter*”) that planetary, regional, and local dynamic analysis could provide in generating lead-time preparedness of a few months to lessen HRI and EHI risk.

Based on historical observations, we can expect a maximum variation in daytime average August WBGT of 3.95°C from the coolest to warmest ENSO quartile (Table 6), which is significant for human health and performance. Historically, high WBGT values in Tokyo are most influenced by La Niña (and both NINO3/3.4 regions). Occasionally, however, an El Niño and neutral phase also explained high WBGT, yet neutral also tends to favor lower WBGT. Further, lead-time information can be found in the Supplemental Material.

Looking toward late summer 2020, the planetary-scale continuation or change of the current neutral ENSO will become clearer as we move closer to August and this spring (MAM). At the urban scale, enhanced daytime thermal exposures are expected, yet with minimal intraurban T_a variation present. Climatology indicates that the August midday T_a in Tokyo will average 30.1°C ($T_{\max} = 31.1^\circ\text{C}$; $T_{\min} = 25.3^\circ\text{C}$), with a high moisture regime that results in daytime *average* WBGT levels of $26.8\text{--}28.6^\circ\text{C}$.

For each outdoor event, the duration, intensity, location, and time of day will be the differentiating factors in lessening EHI and HRI among athletes and attendees. These factors can help operationally in the planning processes for the Games, with potential modifications including:

- Moving the media mix zone to an air-conditioned indoor facility,
- Ensuring adequate airflow to enhance evaporative cooling,
- Utilize on-site monitoring (field, court, track, etc.) for more accurate and timely decision making,
- Increased availability of drinking water and ice,
- Provide free hats and fans for those who are seated in areas with no shade.

These insights can also help inform proactive decision-making for future international events and timing to avoid heat extremes (e.g. Paris 2024 and LA 2028 Olympics; Qatar 2022 (FIFA) and America/Mexico/Canada 2026 (FIFA)). Although Tokyo may face challenges in coping with extreme heat during the Games, they also have an opportunity to adequately prepare and further leave a legacy to enhance Tokyo's urban sustainability, heat mitigation, and citizen health long after the Olympics culminate.

Notes

1. “*Very Strong*” is not part of the official weather service criteria, but is an additional category added in the given analysis based on personal communication with Dr. Jan Null (personal communication), using

the same $+0.5^\circ\text{C}$ increment to capture events that exceeded the “strong” threshold.

2. Note that the logic for retaining WGBT as the “local meteorology” was to identify if previous ENSO season WGBT, namely MAM, could be a predictor for JJA WGBT.
3. Visible Infrared Imaging Radiometer Suite Day-Night Band.
4. NASA’s Moderate Resolution Imaging Spectroradiometer onboard the Terra satellite.
5. Local solar/moisture levels are physically a manifestation of regional circulations impacting on local geography.

Abbreviations

AMeDAS	Automated Meteorological Data Acquisition System
AQMS	Air Quality Monitoring System
AWS	Automatic Weather Station
BOH	Bonin/Ogasawara High
CP	Cerebral palsy
DJF	December, January, February
EHI	Exertional heat illness
ENSO	El Niño Southern Oscillation
HRI	Heat related illness
JJA	June, July, and August
JMA	Japan Meteorological Agency
MAM	March, April, and May
MERRA-2	Modern-Era Retrospective Analysis for Research & Applications
MS	Multiple sclerosis
NCEI	National Centers for Environmental Information
NDVI	Normalized difference vegetation index
NTL	Brightness of nighttime lights
PCA	Principal component analysis
PJI	Pacific Japan Index
PJO	Pacific Japan Oscillation
RFRK	Random forests-based regression kriging
RH	Relative humidity (%)
SCI	Spinal cord injury
SON	September, October, November
SST	Sea-surface temperature ($^\circ\text{C}$)
T_a	Air temperature ($^\circ\text{C}$)
\bar{T}_a	Mean daytime air temperature ($^\circ\text{C}$)
T_{\max}	Daytime high air temperature ($^\circ\text{C}$)
\bar{T}_{\max}	Mean daytime high air temperature ($^\circ\text{C}$)
T_{sfc}	surface temperature ($^\circ\text{C}$)
USGS	U.S. Geological Survey
VSE	Very Strong El Niño (or Super El Niño)
WGBT	Wet bulb globe temperature ($^\circ\text{C}$)
WC	Walker-Circulation
WJ	West-Asia Jet
WJI	West-Asia Jet Index

Acknowledgments

The authors would like to thank Dr. Andrew Perrin for assistance with stochastic modeling; Dr. Walter Kolczynski for support in extracting meta-data files; Dr. Glenn McGregor for very detailed and helpful insight on the analysis and writing; Dr. Jan Null for providing feedback on analysis ideas for ENSO strength; and Dr. Kevin Trenberth, a renowned ENSO expert at the National Center for Atmospheric Research (NCAR), for his time to read and comment on early findings.

Disclosure statement

In accordance with Taylor & Francis policy and my ethical obligation as researchers, the following are potential COIs:

DJC, AJG, YH:

- Have a potential COI as members of the IOC Adverse Weather Impact expert working Group for the Olympic Games Tokyo 2020; not receiving honorarium.

WMT:

- Consultant interest that may arise from the research reported in the enclosed paper. Those interests are fully to Taylor & Francis with an approved plan for managing any potential conflicts arising from this reporting, such as publicly disclosing errors or corrections for the benefit of evolving the science and protecting it from error.

ORCID

Jennifer K. Vanos  <http://orcid.org/0000-0003-1854-9096>
 Andrew J. Grundstein  <http://orcid.org/0000-0002-0574-6253>
 Yuri Hosokawa  <http://orcid.org/0000-0001-9138-5361>
 Ying Liu  <http://orcid.org/0000-0001-5584-7805>
 Douglas J. Casa  <http://orcid.org/0000-0002-8858-2636>

References

- [1] Ashie Y, Kono T. Urban-scale CFD analysis in support of a climate-sensitive design for the Tokyo Bay area. *Int J Climatol*. 2011;31(2):174–188.
- [2] Adachi SA, Kimura F, Kusaka H, et al. Comparison of the impact of global climate changes and urbanization on summertime future climate in the Tokyo metropolitan area. *J Appl Meteorol Climatol*. 2012;51(8):1441–1454.
- [3] Enomoto T, Hoskins BJ, Matsuda Y. The formation mechanism of the Bonin high in August. *Q J R Meteorol Soc*. 2003;129(587):157–178.
- [4] Mulcahy K. Public culture, cultural identity, cultural policy: comparative perspectives. In Galligan A editor. *Patronizing mega-events to globalize identity: the Olympic opening ceremony as a cultural policy*. New York (NY): Palgrave Macmillian; 2017. p. 65–92.
- [5] de Freitas CR, Scott D, McBoyle G. A second generation climate index for tourism (CIT): specification and verification. *Int J Biometeorol*. 2008;52(5):399–407.
- [6] Leyland AA, Howarth HVC, Griffin MJ, et al. Comfortable sardines: the balance between comfort and capacity. 2011.
- [7] Stewart ID, Kennedy CA. Metabolic heat production by human and animal populations in cities. *Int J Biometeorol*. 2016;1–13.
- [8] Hosokawa Y, Grundstein AJ, Casa DJ. Extreme heat considerations in international football venues: the utility of climatologic data in decision making. *J Athl Train*. 2018;53:860–865.
- [9] Gerrett N, Kingma BRM, Sluijter R, et al. Ambient conditions prior to Tokyo 2020 olympic and paralympic games: considerations for acclimation or acclimatization strategies. *Front Physiol*. 2019;10:414.
- [10] Smith KR, Woodward A, Lemke B, et al. The last Summer Olympics? Climate change, health, and work outdoors. *Lancet*. 2016;388(10045):642–644.
- [11] Kosaka E, Iida A, Vanos J, et al. Microclimate variation and estimated heat stress of runners in the 2020 Tokyo Olympic Marathon. *Atmosphere*. 2018;9(5). DOI:10.3390/atmos9050192
- [12] Matzarakis A, Fröhlich D, Bermon S, et al. Quantifying thermal stress for sport events—the case of the Olympic Games 2020 in Tokyo. *Atmosphere*. 2018;9(12):479.
- [13] Kakamu T, Wada K, Smith DR, et al. Preventing heat illness in the anticipated hot climate of the Tokyo 2020 Summer Olympic Games. *Environ Health Prev Med*. 2017;22(1):68.
- [14] Peiser B, Reilly T. Environmental factors in the summer Olympics in historical perspective. *J Sports Sci*. 2004;22(10):981–1002.
- [15] Roth M. Review of urban climate research in (sub) tropical regions. *Int J Climatol*. 2007;27(14):1859–1873.
- [16] Vanos JK, Kosaka E, Iida A, et al. Planning for spectator thermal comfort and health in the face of extreme heat: the Tokyo 2020 Olympic marathons. *Sci Total Environ*. 2019;657:904–917.
- [17] International Paralympic Committee. Tokyo 2019 Paralympic Games.
- [18] Griggs KE, Stephenson BT, Price MJ, et al. Heat-related issues and practical applications for Paralympic athletes at Tokyo 2020. *Temperature* 2019;7(1):37–57. (just-accepted). doi: 10.1080/23328940.2019.1617030.
- [19] Meehan P, Toomey KE, Drinnon J, et al. Public health response for the 1996 Olympic Games. *Jama*. 1998;279(18):1469–1473.
- [20] Honjo T, Seo Y, Yamasaki Y, et al. Thermal comfort along the marathon course of the 2020 Tokyo Olympics. *Int J Biometeorol*. 2018;62(8):1407–1419.
- [21] Nitta T, Motoki T. Abrupt enhancement of convective activity and low-level westerly burst during the onset

- phase of the 1986–87 El Niño. *J Meteorol Soc Japan Ser II*. 1987;65(3):497–506.
- [22] Wakabayashi S, Kawamura R. Extraction of major teleconnection patterns possibly associated with the anomalous summer climate in Japan. *J Meteorol Soc Japan Ser II*. 2004;82(6):1577–1588.
- [23] Kawamura R, Ogasawara T. On the role of typhoons in generating PJ teleconnection patterns over the western North Pacific in late summer. *SOLA*. 2006;2:37–40.
- [24] Bjerknes J. Atmospheric teleconnections from the equatorial Pacific. *Mon Weather Rev*. 1969;97(3):163–172.
- [25] Barnston AG, Glantz MH, He Y. Predictive skill of statistical and dynamical climate models in SST forecasts during the 1997–98 El Niño episode and the 1998 La Niña onset. *Bull Am Meteorol Soc*. 1999;80(2):217–244.
- [26] Trenberth KE, Stepaniak DP. Indices of el niño evolution. *J Clim*. 2001;14(8):1697–1701.
- [27] Rasmusson EM, Carpenter TH. Variations in tropical sea surface temperature and surface wind fields associated with the Southern Oscillation/El Niño. *Mon Weather Rev*. 1982;110(5):354–384.
- [28] McGregor GR, Ebi K. El Niño Southern Oscillation (ENSO) and health: an overview for climate and health researchers. *Atmosphere*. 2018;9(7):282.
- [29] Lam HCY, Haines A, McGregor G, et al. Time-series study of associations between rates of people affected by disasters and the El Niño Southern Oscillation (ENSO) cycle. *Int J Environ Res Public Health*. 2019;16(17):3146.
- [30] American Meteorological Society. AMS glossary - “teleconnection”. AMS Glossary
- [31] Nitta T. Convective activities in the Tropical Western Pacific and their impact on the northern hemisphere summer circulation. *J Meteorol Soc Japan Ser II*. 1987;65(3):373–390.
- [32] Hanley DE, Bourassa MA, O’Brien JJ, et al. A quantitative evaluation of ENSO indices. *J Clim*. 2003;16(8):1249–1258.
- [33] Nitta T. Global features of the Pacific–Japan oscillation. *Meteorol Atmos Phys*. 1989;41(1):5–12.
- [34] Urabe Y, Maeda S. The relationship between Japan’s recent temperature and decadal variability. *Sola*. 2014;10:176–179.
- [35] Trenberth KE. The definition of el niño. *Bull Am Meteorol Soc*. 1997;78(12):2771–2778.
- [36] Holland GJ. Predicting el Niño’s impacts. *Science*. 2009;325(5936):47.
- [37] NOAA. El Niño/Southern Oscillation (ENSO) Diagnostic Discussion; 2019 [cited 2019 Oct 23]. Available from: https://www.cpc.ncep.noaa.gov/products/analysis_monitoring/enso_advisory/ensodisc.shtml
- [38] APCC APEC Climate Center. Climate information services. *Seasonal Forecast*; 2020 [cited 2020 Jan 20]. Available from: <https://apcc21.org/ser/outlook.do?lang=en>
- [39] Krishnan R, Sugi M. Baiu rainfall variability and associated monsoon teleconnections. *気象集誌 第2輯*. 2001;79(3):851–860.
- [40] Vega A, Du-penhoat Y, Dewitte B, et al. Equatorial forcing of interannual Rossby waves in the eastern South Pacific. *Geophys Res Lett*. 2003;30(5). DOI:10.1029/2002GL015886
- [41] Qu X, Huang G. Impacts of tropical Indian Ocean SST on the meridional displacement of East Asian jet in boreal summer. *Int J Climatol*. 2012;32(13):2073–2080.
- [42] Tsuyuki T, Kurihara K. Impact of convective activity in the western tropical Pacific on the East Asian summer circulation. *J Meteorol Soc Japan Ser II*. 1989;67(2):231–247.
- [43] Yunus AP, Dou J, Sravanthi N. Remote sensing of chlorophyll-a as a measure of red tide in Tokyo Bay using hotspot analysis. *Remote Sens Appl Soc Environ*. 2015;2:11–25.
- [44] NOAA/NCEP Climate Prediction Center. El Niño Southern Oscillation: NINO3 and NINO3.4 Indicators. *Teleconnections*; 2019 [cited 2019 Aug 20]. Available from: <https://www.ncdc.noaa.gov/teleconnections/enso/indicators/sst/>
- [45] Kalnay E, Kanamitsu M, Kistler R, et al. The NCEP/NCAR 40-year reanalysis project. *Bull Am Meteorol Soc*. 1996;77(3):437–472.
- [46] NOAA ESRL. El Niño Southern Oscillation (ENSO): top 24 strongest El Niño and La Niña events by season;2018
- [47] IITM. Interannual variations of indian summer monsoon; 2017 [cited 2019 May 20]. Available from: <https://www.tropmet.res.in/~kolli/MOL/Monsoon/Historical/air.html>
- [48] NASA. MERRA-2: file specification. *GMAO office note No. 9 (version 1.1)*. Global Modeling and Assimilation Office Website. <https://gmao.gsfc.nasa.gov/pubs/docs/Bosilovich785.pdf>
- [49] Yato H, Nomura Y, Umehara K, et al. Automated Meteorological Data Acquisition System (AMeDAS) in Japan and field experiments to determine the effects of its observation environment. In: WMO, editors. *WMO International Conference on Automatic Weather Stations (ICAWS-2017)*; Offenbach am Main, Germany; 2017.p. 1–7.
- [50] Meisei. Sensing & communication. Japan; 2017.
- [51] Noguchi T, Yamanaka T, Nakatsugawa A. Automated Meteorological Data Acquisition System (AMEDAS). *JAPAN Telecommun Rev*. 1975;17(1):45–53.
- [52] Liljegren JC, Carhart RA, Lawday P, et al. Modeling the wet bulb globe temperature using standard meteorological measurements. *J Occup Environ Hyg*. 2008;5(10):645–655.
- [53] Patel T, Mullen SP, Santee WR. Comparison of methods for estimating wet-bulb globe temperature index from standard meteorological measurements. *Mil Med*. 2013;178(8):926–933.
- [54] Budd GM. Wet-bulb globe temperature (WBGT) - its history and its limitations. *J Sci Med Sport*. 2008;11(1):20.
- [55] McGregor GR, Vanos JK. Heat: a primer for public health researchers. *Public Health*. 2018;161:138–146.
- [56] Havenith G, Fiala D. Thermal indices and thermophysiological modeling for heat stress. *Compr Physiol*. 2016;6:255–302.

- [57] Minard D. Prevention of heat casualties in Marine Corps recruits: period of 1955–60, with comparative incidence rates and climatic heat stresses in other training categories. *Mil Med.* 1961;126(4):261–272.
- [58] Schickele E. Environment and fatal heat stroke: an analysis of 157 cases occurring in the army in the US during World War II. *Mil Surg.* 1947;100(3):235–256.
- [59] Yaglou CP, Minard D. Control of heat casualties at military training centers. *AMA Arch Ind Heal.* 1957;16(4):302.
- [60] Houssein M, Lopes P, Fagnoni B, et al. Hydration: the new FIFA world cup's challenge for referee decision making? *J Athl Train.* 2016;51(3):264–266.
- [61] Hosokawa Y, Casa D, Vanos JK, et al. Activity modification in heat: critical assessment of guidelines across athletic, occupational, and military settings. *Int J Biometeorol.* 2019;63(3):405–427.
- [62] Armstrong LE, Casa DJ, Millard-Stafford M, et al. Exertional heat illness during training and competition. *Med Sci Sports Exerc.* 2007;39(3):556–572.
- [63] Casa DJ, DeMartini JK, Bergeron MF, et al. National Athletic Trainers' Association position statement: exertional heat illnesses. *J Athl Train.* 2015;50(9):986–1000.
- [64] Richman MB. Rotation of principal components. *J Climatol.* 1986;6(3):293–335.
- [65] Hengl T, Heuvelink GBM, Kempen B, et al. Mapping soil properties of Africa at 250 m resolution: random forests significantly improve current predictions. *PLoS One.* 2015;10(6):e0125814.
- [66] Liu Y, Cao G, Zhao N, et al. Improve ground-level PM2.5 concentration mapping using a random forests-based geostatistical approach. *Environ Pollut.* 2018;235:272–282.
- [67] NASA. MODIS level-3 vegetation indices and land surface temperature products;2019.
- [68] NCEI. Version 1 VIIRS day/night band nighttime lights;2019. https://ngdc.noaa.gov/eog/viirs/download_dnb_composites.html
- [69] Vancutsem C, Ceccato P, Dinku T, et al. Evaluation of MODIS land surface temperature data to estimate air temperature in different ecosystems over Africa. *Remote Sens Environ.* 2010;114(2):449–465.
- [70] Hardin AW, Liu Y, Cao G, et al. Urban heat island intensity and spatial variability by synoptic weather type in the northeast US. *Urban Clim.* 2018;24:747–762.
- [71] Marlon JR, Bartlein PJ, Carcaillet C, et al. Climate and human influences on global biomass burning over the past two millennia. *Nat Geosci.* 2008;1(10):697.
- [72] Brown RD, Gillespie TJ. Microclimate landscape design. John Wiley & Sons, Inc.; 1995.
- [73] Hosokawa Y, Grundstein AJ, Vanos JK, et al. Environmental condition and monitoring. In Casa D editor. *Sport and physical activity in the heat.* Springer, Cham; 2018. p. 147–162.
- [74] Kosaka Y, Nakamura H. A comparative study on the dynamics of the Pacific-Japan (PJ) teleconnection pattern as revealed in reanalysis datasets. 2008.
- [75] Deser C, Phillips AS, Alexander MA, et al. Projecting North American climate over the next 50 years: uncertainty due to internal variability. *J Clim.* 2014;27(6):2271–2296.
- [76] Solís P, Vanos JK, Forbis RE. The decision-making/accountability spatial incongruence problem for research linking environmental science and policy. *Geogr Rev.* 2017;107(4):680–704.
- [77] Snowise M, Dexter WW, Dexter WW, et al. Sun exposure: managing—and preventing—skin damage. *Phys Sportsmed.* 2004;32(12):26–32.
- [78] Downs NJ, Axelsen T, Schouten P, et al. Biologically effective solar ultraviolet exposures and the potential skin cancer risk for individual gold medalists of the 2020 Tokyo Summer Olympic Games. *Temperature.* 2019;7(1):89–108. doi: 10.1080/23328940.2019.1581427.
- [79] Aburto-Corona J, Aragón-Vargas L. Sunscreen use and sweat production in men and women. *J Athl Train.* 2016;51(9):696–700.
- [80] Martin DE. Strategies for optimising marathon performance in the heat. *Sport Med.* 2007;37(4–5):324–327.
- [81] Pandolf KB, Gange RW, Latzka WA, et al. Human thermoregulatory responses during cold water immersion after artificially induced sunburn. *Am J Physiol Integr Comp Physiol.* 1992;262(4):R617–R623.
- [82] Normell LA. Distribution of impaired cutaneous vasomotor and sudomotor function in paraplegic man. *Scand J Clin Lab Invest.* 1974;53(138):25–41.
- [83] Freund PR, Brengelmann GL, Rowell LB, et al. Attenuated skin blood flow response to hyperthermia in paraplegic men. *J Appl Physiol.* 1984;56(4):1104–1109.
- [84] Hopman MTE. Circulatory responses during arm exercise in individuals with paraplegia. *Int J Sports Med.* 1994;15:126–131.
- [85] Binkhorst RA, Oeseburg B, Hopman MTE. Cardiovascular responses in paraplegic subjects during arm exercise. *Eur J Appl Physiol Occup Physiol.* 1992;65(1):73–78.
- [86] Veltmeijer MT, Pluim B, Thijssen DH, et al. Thermoregulatory responses in wheelchair tennis players: a pilot study. *Spinal Cord.* 2014;52(5):373.
- [87] Girard O. Thermoregulation in wheelchair tennis—how to manage heat stress? *Front Physiol.* 2015;6:175.
- [88] Maltais D, Wilk B, Unnithan V, et al. Responses of children with cerebral palsy to treadmill walking exercise in the heat. *Med Sci Sports Exerc.* 2004;36(10):1674–1681.
- [89] Runciman P, Tucker R, Ferreira S, et al. Paralympic athletes with cerebral palsy display altered pacing strategies in distance-deceived shuttle running trials. *Scand J Med Sci Sports.* 2016;26(10):1239–1248.
- [90] Davis SL, Wilson TE, White AT, et al. Thermoregulation in multiple sclerosis. *J Appl Physiol.* 2010;109(5):1531–1537.
- [91] Bongers CCWG, Hopman MTE, Eijsvogels TMH. Cooling interventions for athletes: an overview of effectiveness, physiological mechanisms, and practical considerations. *Temperature.* 2017;4(1):60–78. doi: 10.1080/23328940.2016.1277003.